Calculation of heavy quark production in electron-positron and photon-photon collision using the k_t-factorization approach

M. Hansson, H. Jung and L. Jönsson

Department of Physics
Lund University, Lund, Sweden

Abstract

The production cross section of heavy quarks in real and virtual photon-photon collisions has been studied. The unintegrated gluon density in the photon was obtained using the CCFM evolution equation for the first time. The gluon density was implemented in the Monte Carlo generator CASCADE, and cross sections for heavy quark production in e^+e^- collisions were calculated and compared to LEP data. Also, predictions for heavy quark cross sections in e^+e^- and $\gamma\gamma$ collisions at TESLA energies are given.

1 Introduction

The production of heavy flavour (b and c quarks) in $\gamma\gamma$ collisions has been studied at LEP [1, 2, 3, 4, 5, 6, 7, 8, 9, 10] for many years and will be an important field of study at TESLA [11, 12]. It has also been studied in proton-photon collision at HERA [13, 14, 15, 16, 17, 18], and in proton-proton collisions at the TEVATRON [19, 20, 21, 22]. Whereas the measured charm cross sections are well described by the parton evolution according to the standard collinear approach, the measured beauty cross sections are a factor 2-4 larger than predictions. However, by using so called k_t-factorization and an unintegrated gluon density for the proton, the beauty cross sections are now in good agreement with data in pp collisions [23, 24]. The aim of this paper is to investigate if the $b\bar{b}$ cross section also can be explained in $\gamma\gamma$ collisions by using k_t- factorization and an unintegrated gluon density for the photon.

The structure function of the photon can be written as

$$F_2^\gamma(x,\mu^2) = x\sum_i e_i^2 f_i^\gamma(x,\mu^2)$$

where e_i is the electric charge of parton i and one sums over all quark flavours. In general, the cross section for a parton i from one photon to interact with a parton j from another photon and form the final state X is

$$\sigma = \sum_{i,j}\int \frac{dx_1}{x_1}\frac{dx_2}{x_2}\cdot f_i^\gamma(x_1,\mu^2)\cdot f_j^\gamma(x_2,\mu^2)\cdot \hat{\sigma}_{i+j\to X}(x_1,x_2,s) \tag{1}$$

where the parton densities f_i^γ and f_j^γ describe the probability of finding partons i and j with momentum fractions x_1 and x_2 and the partonic cross section $\hat{\sigma}$ describes the probability that the two particles i and j will create the final state X.

2 k_t-factorization

In equation (1) all partons are assumed to travel in the same direction as the incoming particle, i.e. they have no transverse momenta. This is therefore called a collinear approximation. However, at large energies, where small x gluons are probed, the transverse momenta, k_t, of the partons are expected to become important. Therefore, the cross sections are factorized [25, 26, 27, 28] into a k_t-dependent partonic cross section $\hat{\sigma}(x, k_t^2, \mu^2)$, where the incoming partons are treated off-mass shell, and a k_t-dependent parton density function $\mathcal{A}(x, k_t^2, \mu^2)$. The equivalent to equation (1) then becomes

$$\sigma = \sum_{i,j} \int \frac{dx_1}{x_1} \frac{dx_2}{x_2} dk_{t1}^2 dk_{t2}^2 \mathcal{A}_i^\gamma(x_1, k_{t1}^2, \mu^2) \mathcal{A}_j^\gamma(x_2, k_{t2}^2, \mu^2) \hat{\sigma}_{i+j\to X}(k_{t1}, k_{t2}, x_1, x_2, s). \qquad (2)$$

The function $\mathcal{A}(x, k_t^2, \mu^2)$ is called the (k_t-) unintegrated gluon density and is related to the collinear one by

$$g(x, \mu^2) \simeq \int_0^{\mu^2} dk_t^2 \mathcal{A}(x, k_t^2, \mu^2), \qquad (3)$$

where $\mathcal{A}(x, k_t^2, \mu^2)$ describes the probability to find a gluon with a longitudinal momentum fraction x and a transverse momentum k_t at a scale μ^2. Inverting the relation (3) gives that an unintegrated gluon density may be obtained by differentiating an integrated gluon density with respect to μ^2,

$$\mathcal{G}(x, k_t^2) \equiv \left. \frac{dg(x, \mu^2)}{d\mu^2} \right|_{\mu^2 = k_t^2}. \qquad (4)$$

Note that the unintegrated gluon density obtained in this way only depends on one scale, since $\mu^2 = k_t^2$. To distinguish the different parton distributions, the notation following [29] is used: $g(x, \mu^2)$ is the parton distribution in the collinear approach, while $\mathcal{G}(x, k_t^2)$ and $\mathcal{A}(x, k_t^2, \mu^2)$ are the one- and two-scale distributions in the k_t-factorization approach. When using off-shell matrix elements of leading order ($O(\alpha_s)$), some next-to leading order ($O(\alpha_s^2)$) processes in the collinear approach are effectively included, in addition to all collinear leading order processes.

3 Heavy quark production processes

Heavy quark production in photon collisions can be explained by three mechanisms, shown in Figure 1. At small $\sqrt{s}$, the cross section is dominated by the direct part (a-c). In this case, the photons couple directly to the quarks, and the process is therefore not dependent on the quark and gluon content in the photon. Hence, the lowest, or zeroth, order process (a) can be calculated in pure QED, while first order corrections, including real (b) and virtual (c) gluon radiation, also depend on the QCD coupling constant. These corrections have been calculated in [30] and were found to contribute 30% of the cross section in the direct case. It has also been shown that the direct part alone (including corrections) cannot reproduce the measurements of b and c quark production in e^+e^-, ep and pp collisions.

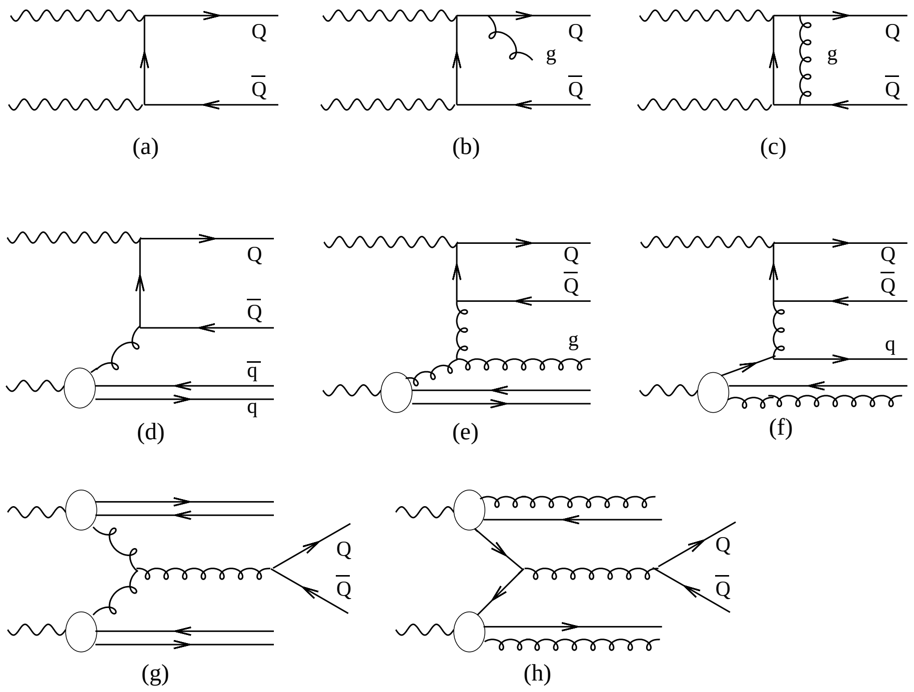

Figure 1: *Production mechanisms in heavy quark production.*

The direct (a-c) and single resolved processes (d-f) are predicted to give equal contributions to the cross section at $\sqrt{s} \approx 200$ GeV [30]. The double resolved case (g-h) gives a smaller contribution than the direct and single resolved processes, since it depends on α^2, but it becomes increasingly important with increasing energy.

In e^+e^- reactions there are additional contributions to heavy quark production, which have been discussed in [31]. The most important contribution comes from initial or final state radiation of a γ^*/Z, which decays into a heavy quark pair. The cross section of other processes discussed in [31] are typically several orders of magnitude smaller at linear collider energies. Only the diagrams shown in Figure 1a, d, e and g have been taken into account in this analysis.

4 Higher order processes

The processes in Figure 1 are all of zeroth, first or second order in the strong coupling α_s. In order to take higher order corrections into account evolution equations are used. The general structure of an evolution equation is

$$f_j = f_0 + \int f_i \cdot P_{i \to j,k}$$

where f_i and f_j are the parton density functions for the mother and daughter propagator gluons, f_0 is the input gluon density function and $P_{i \to j,k}$ is the splitting kernel describing the probability that the parton i is split into two partons j and k. In the following discussion, the evolution starts at the bottom in Figure 2 and continues towards the

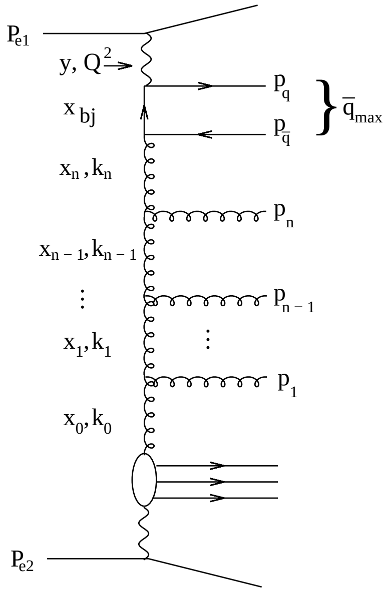

Figure 2: *Parton ladder created by gluon emissions.*

quark box. The possible splittings are $q \to qg$, $g \to q\bar{q}$ and $g \to gg$. There are a number of different evolution equations, each one taking different parts of the full calculation into account and evolving the density functions in different variables. A short presentation of three different approaches follows, where the first is valid for large μ^2, the second is valid for small x and moderate μ^2, and the third is valid for both these regions. The latter is of special importance for this paper.

4.1 The DGLAP evolution

The DGLAP [32, 33, 34, 35] evolution equation is of the form

$$\frac{df_j(x,\mu^2)}{d\ln\mu^2} = \frac{\alpha_s(\mu^2)}{2\pi}\sum_i \int_x^1 \frac{dx'}{x'} f_i(x',\mu^2) P_{i\to j,k}(z) \tag{5}$$

where $f(x,\mu^2)$ is the density of partons carrying a longitudinal momentum fraction x probed at a scale μ^2, and $P_{i\to j,k}(z)$ describes the probability that a parton i is split into two partons j and k with a fraction $z = \frac{x}{x'}$ and $1-z$ of the original parton momentum, respectively. The probability that a gluon splits into two gluons is given by

$$P_{g\to g,g}(z) = \frac{1}{1-z} - 2 + z(1-z) + \frac{1}{z} \tag{6}$$

where the terms $\frac{1}{1-z}$ and $\frac{1}{z}$ are called the singular terms, since they give infinite contributions when $z \to 1$ and $z \to 0$, respectively. The equation (5) thus describes the probability change of finding a parton of type j with momentum fraction x as we increase the scale μ^2. In the DGLAP formalism, the gluon chain in Figure 2 is assumed to be strongly ordered in virtuality

$$\mu^2 \gg |k_n^2| \ldots \gg |k_1^2| \gg |k_0^2|, \tag{7}$$

where k_i is the four momentum of parton i. It can be shown that the ordering in virtuality implies that also the transverse momentum of the propagator partons are strongly ordered (at small z) according to

$$\mu^2 \gg |k_{tn}^2| \ldots \gg |k_{t1}^2| \gg |k_{t0}^2| \quad (8)$$

Since the virtualities and transverse momenta of the gluon propagators are small compared to the hard scale, μ^2, they can be treated as massless and approximated to move in the same direction as the incoming proton (collinear approximation). It can be shown, that the DGLAP evolution gives a resummation of terms of the form $(\alpha_s \ln(\mu^2))^n$ in the expansion of the cross section. Hence, the DGLAP approximation is only valid at large μ^2 where these terms will dominate.

4.2 The BFKL evolution

The BFKL [36, 37, 38] evolution equation resums the terms $(\alpha_s \ln(\frac{1}{x}))^n$ in the expansion, and is thus only valid at small x. Consequently, the evolution is made in increasing $\ln(\frac{1}{x})$, since

$$x_0^2 \gg x_1^2 \ldots \gg x_n^2 \gg x_{Bj}^2 \quad (9)$$

has been assumed. This implies that the emitted gluons will take a large fraction of the propagator momentum. However, there is no restriction in k^2 or k_t^2. This means that the virtualities and transverse momenta of the propagators can take any kinematically allowed value and must not be smaller than the photon virtuality as was the case in the DGLAP description. Consequently the collinear approach is no longer applicable but the matrix elements must be taken off mass shell (the particles can have virtual mass) and unintegrated parton densities, taking the transverse momenta of the propagators into account, have to be used. The BFKL evolution equation is of the form

$$\frac{d\mathcal{G}(x, k_t^2)}{d\ln(\frac{1}{x})} = \int dk_t'^2 \mathcal{G}(x, k_t'^2) \cdot K(k_t^2, k_t'^2) \quad (10)$$

where $\mathcal{G}(x, k_t^2)$ was defined by eq. (4). The function K is the splitting kernel equivalent to P in (5).

4.3 The CCFM evolution

The CCFM [39, 40, 41, 42] evolution equation is valid both at large and small x, since it resums terms of both the form $(\alpha_s \ln(\frac{1}{x}))^n$ and $(\alpha_s \ln(\frac{1}{1-x}))^n$. This means that at large x the CCFM evolution will be DGLAP-like, and at small x it will be BFKL-like. The CCFM evolution includes angular ordering in the initial state cascade, which means that the emission angles of the partons with respect to the propagator increases as one moves towards the quark box,

$$\Xi \gg \xi_n \gg \ldots \xi_1 \gg \xi_0, \quad (11)$$

where the maximum allowed angle Ξ is set by the hard quark box.

The original CCFM splitting function $\tilde{P}$ was defined as

$$\tilde{P}_g(z, k_t^2, \bar{q}) = \frac{\bar{\alpha}_s(\bar{q}_i^2)}{1 - z_i} + \frac{\bar{\alpha}_s(k_{ti}^2)}{z_i} \Delta_{ns}(z_i, k_{ti}^2, \bar{q}_i^2), \quad (12)$$

where

$$\bar{q}_i = \frac{p_{ti}}{1 - z_i} = x_{i-1}\sqrt{s\xi_i}$$

is the rescaled transverse momentum of the emitted gluon i and $z_i = \frac{x_i}{x_{i-1}}$. The CCFM splitting function differs from the DGLAP splitting function in the sense that it only includes the singular terms. Another difference is the additional function Δ_{ns}, called the non-Sudakov form factor. The non-Sudakov form factor originates from the fact that, in CCFM and BFKL, all virtual corrections in the gluon vertex are automatically taken into account. This is called the Reggeization of the gluon vertex.

At very high energies the $1/z$-term in the splitting function will dominate and it is sufficient to include the singular terms. However, for the energies at present colliders it is still necessary to take the non-singular terms into account in the splitting function, which then takes the form:

$$\begin{aligned} \tilde{P}_g(z, k_t^2, \bar{q}) &= \bar{\alpha}_s(\bar{q}_i^2)\left(\frac{z_i}{1 - z_i} + \frac{z_i(1 - z_i)}{2}\right) \\ &\quad + \bar{\alpha}_s(k_{ti}^2)\left(\frac{(1 - z_i)}{z_i} + \frac{z_i(1 - z_i)}{2}\right)\Delta_{ns} \end{aligned} \tag{13}$$

In this study the splitting function given by eq(12) was used.

5 Monte Carlo simulations

The Monte Carlo generator CASCADE [43] is based on the CCFM evolution equation and thus uses unintegrated parton desities and off-shell matrix elements. For technical reasons, a backward evolution is used, where first the hard scattering is generated and then the initial state cascade (the gluon ladder) is evolved from the quark box to the incoming particles. In this evolution only gluon emissions are treated, that is, only the splitting $g \to gg$ is considered. CASCADE also performs the hadronization, using the Lund string model in JETSET/PYTHIA [44].

6 The unintegrated gluon density

The evolution of the unintegrated gluon density was made using the CCFM equation in a forward evolution procedure based on the Monte Carlo technique as described in [46]. An initial gluon distribution is chosen as well as a starting scale μ_s and a rescaled transverse momentum $\bar{q}_s$, which is related to the emission angle for the first emitted gluon. The default values $\mu_s = \bar{q}_s = 1.4$ GeV was obtained by a fit to the proton structure function [46]. The evolution then starts with $\bar{q}_{max,0} = \bar{q}_s$, and k_{t0} chosen from a Gaussian distribution around μ_s to simulate a Fermi motion of the partons. x_0 is chosen from the initial gluon distribution using the Monte Carlo method. The branching is then repeated until the next emitted gluon would have a higher $\bar{q}$ than $\bar{q}_{max,0}$. This is repeated 10^7 times for each of 50 different maximum $\bar{q}_{max,i}$ chosen from $\bar{q}_{max,0} = \bar{q}_s < \bar{q}_{max,i} < \bar{q}_{max,50} = 1800$ GeV in steps of $log(\bar{q}_{max})$, thus giving a distribution $\mathcal{A}(x, k_t^2, \bar{q}^2)$ in a $50 \times 50 \times 50$ grid of $log(x)$, $log(k_t^2)$

and $log(\bar{q}_{max})$. For values between the gridpoints the method of linear interpolation is used. With the unintegrated parton distribution avaliable, a backward evolution scheme can be used for the simulation of the parton emissions.

6.1 One-loop evolution

To make sure that the evolution procedure is working, the evolution was first made for the proton with a GRV[1] input distribution (using the default values $\mu_s = \bar{q}_s = 1.4$ GeV) and using the one-loop approximation [47, 48, 49], which means that the CCFM evolution is reduced to the DGLAP evolution, with the difference that the CCFM one-loop evolution still treats the full kinematics, i.e. it takes the transverse momentum k_t into account. This is done by putting $\Delta_{ns} = 1$ in the splitting function and reducing angular ordering to ordering in transverse momentum. The obtained distribution $x\mathcal{A}(x, k_t^2, \bar{q}^2)$ was then integrated over k_t^2,

$$\int_0^{\bar{q}^2} dk_t^2 x\mathcal{A}(x, k_t^2, \bar{q}^2) = x\mathcal{G}(x, \bar{q}^2), \tag{14}$$

and compared to the original GRV distribution at different scales, see Figure 3. The small

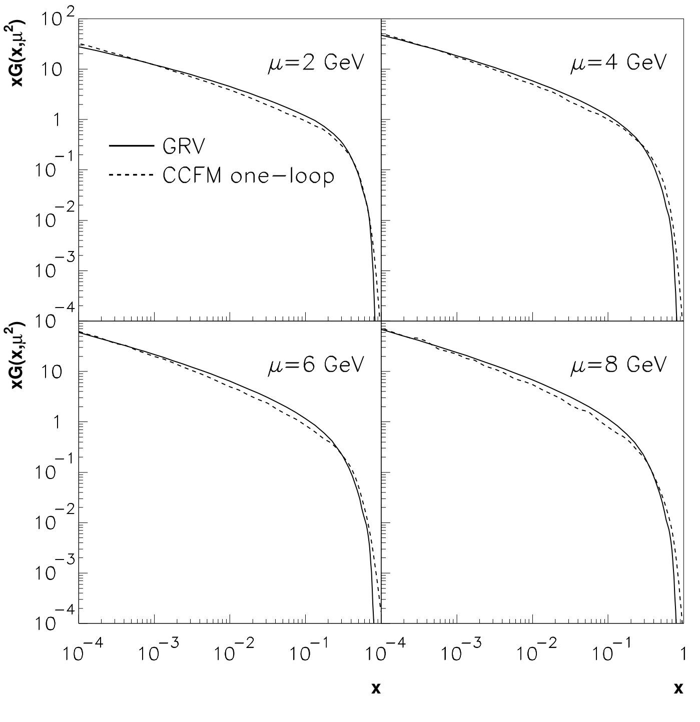

Figure 3: *The integrated CCFM one-loop evolved distribution for the proton compared to the GRV distribution at different scales.*

differences are due to the fact that the splitting function only contains the singular parts,

[1]GRV 98 LO was used

and that only the splitting $g \to gg$ is considered. Nevertheless, the distributions are still in good agreement which indicates that the evolution machinery is working.

The situation for the photon is a bit different, since the structure function, in addition to the hadronic component, now also consists of a pointlike component which reflects the splitting of the photon into a quark-antiquark pair. In addition, there are no sum rules equivalent to those in the proton case that constrain the quark distributions in the photon. However, these differences do not matter, since we only use the gluon distribution and the gluon splitting $g \to gg$. Figure 4 shows the evolved distribution for the photon, using the same parameters as in the proton case and the GRV[2] as input distribution, compared to the input distribution at different scales. The one-loop evolved and the GRV distribution are similar, although the one-loop evolved distribution is a bit steeper at large scales. It is not surprising that the one-loop evolution does not give equally good agreement in the proton and the photon case, since the same parameters have been used in both one-loop evolutions, while different techniques and starting scales for the proton and the photon were used to obtain the original GRV distributions.

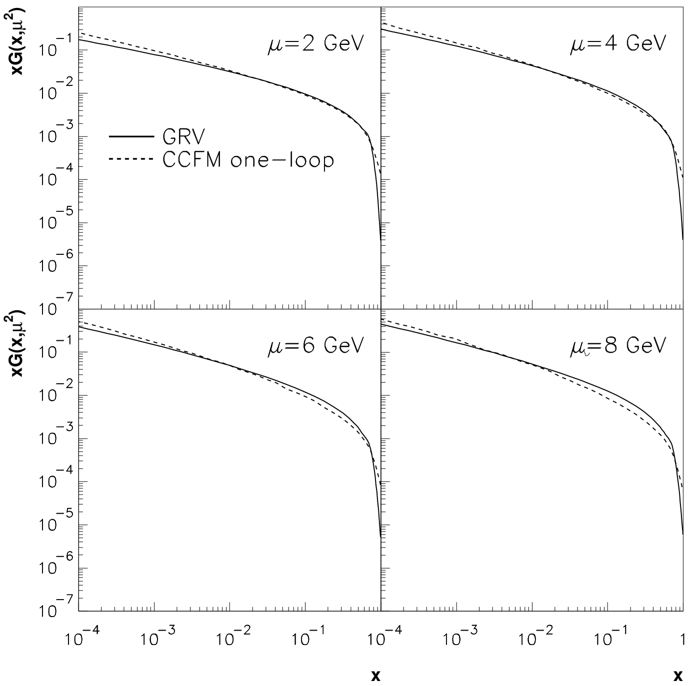

Figure 4: *The integrated CCFM one-loop evolved distribution for the photon compared to the GRV distribution at different scales.*

¿From the above we conclude that the one-loop evolution is able to reproduce the input distributions reasonably well, and hence that the evolution machinery is working for the CCFM one-loop case. A similar test cannot be done for the full CCFM evolution,

[2]GRV-G LO was used

since the obtained distributions should be different from the ones obtained with CCFM one-loop evolution. However, it has already been shown [46] that the CCFM evolution is working for the proton, in the sense that it can explain data, for example $b\bar{b}$ production at the TEVATRON, which could not be explained with other methods. Since the only difference between the photon and proton evolution is the starting distribution, it can be assumed that the CCFM evolution will work also for the photon.

6.2 Full CCFM evolution

After making sure that the parton evolution scheme gives consistent results, the unintegrated gluon density for the photon was evolved using the full CCFM evolution procedure. The obtained distributions integrated over k_t^2 are compared in Figure 5 to the GRV[3] distribution, which was used as input distribution. One of the more obvious differences is that the CCFM evolved distribution is much higher than the original GRV. This is due to differences in the definition of the integrated gluon density; one can either integrate over d^2k_t or over dk_t^2. The difference is a factor π, which explains the main part of the normalization difference. We can also note that the CCFM evolved distribution is less steep than the original GRV. This is a consequence of that the non-Sudakov form factor $\Delta_{ns} \to 0$ when $z \to 0$ and thereby screens the $\frac{1}{z}$ factor in the splitting function. This results in a lower splitting probability compared to the DGLAP case (where $\Delta_{ns} = 1$) which becomes visible in the small x (small z) region where the factor $\frac{1}{z}$ dominates the splitting function.

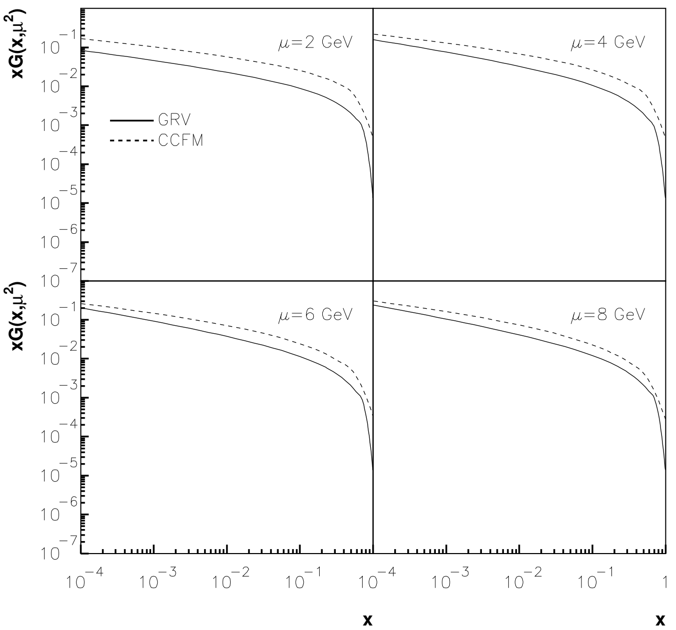

Figure 5: *The integrated CCFM evolved distribution for the photon compared to the GRV distribution at different scales.*

[3]GRV-G HO was used

6.3 Uncertainties

In the evolution of the unintegrated gluon distributions above, the GRV density was used as input distribution, with $\mu_s = \bar{q}_s = 1.4$ GeV given from a fit to the parton density of the proton [46]. The question is how sensitive the results are to the selected starting distribution and the parameters chosen. Therefore, the evolution was made also with the SaS[4] [50] parton distribution as input (and keeping $\mu_s = \bar{q}_s = 1.4$ GeV), and also with the GRV parametrization as input but with $\mu_s = 1.4$ GeV and $\bar{q}_s = 1.2$ GeV, $\mu_s = 1.4$ GeV and $\bar{q}_s = 1.6$ GeV, and $\mu_s = 1$ GeV and $\bar{q}_s = 1.4$ GeV. The various distributions obtained are compared to the previous ones in Figure 6. We notice that there is only a weak dependence on the starting value $\bar{q}_s$, such that the distribution becomes somewhat flatter at large $\bar{q}_s$. This can be understood, since a larger starting angle would mean that it takes less emissions to reach the maximum value (since there is angular ordering), and less emissions would mean that the gluon entering the matrix element (gluon n in Figure 2) would have a larger longitudinal momentum fraction x. A change in μ_s makes a significant difference, where a smaller μ_s gives a distribution which is lower at small x. One can also see that the evolution depends on the choice of input distribution, where the main features of the input distribution remains after the evolution, see also Figure 7.

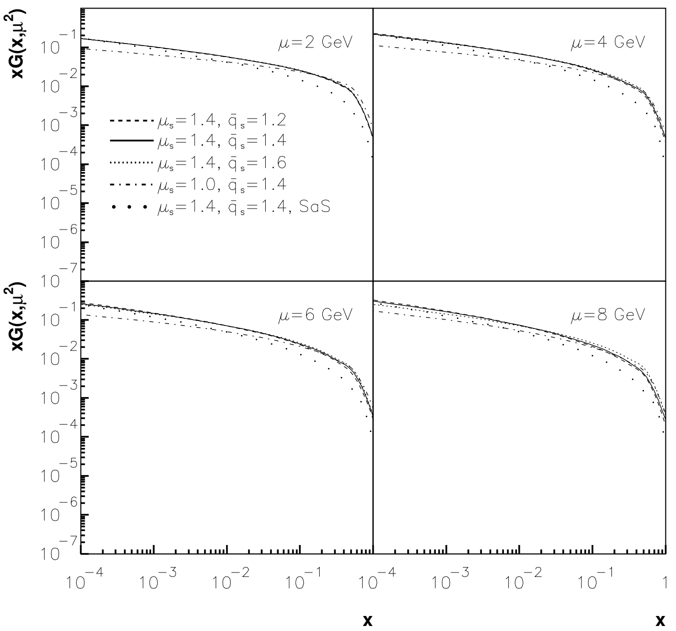

Figure 6: *The integrated CCFM evolved distributions for the photon with different combinations of μ_s, $\bar{q}_s$ and input distributions.*

[4]SaS-G 1D was used

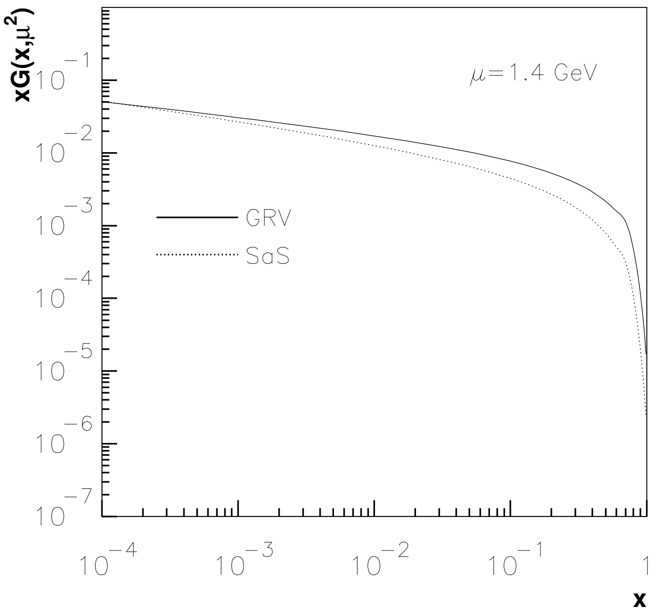

Figure 7: *The GRV and SaS distributions compared at the starting scale $\mu = 1.4$ GeV.*

7 Heavy quark cross sections

The heavy quark cross sections in e^+e^- collisions can be calculated using the relation

$$\sigma_{e^+e^-\to e^+e^-b\bar{b},c\bar{c}X} = \int \frac{dQ_1^2}{Q_1^2}\frac{dQ_2^2}{Q_2^2}\mathcal{L}_{\gamma\gamma}(W_{\gamma\gamma},Q_1^2,Q_2^2)\sigma_{\gamma\gamma\to b\bar{b},c\bar{c}X}(W_{\gamma\gamma})dW_{\gamma\gamma} \tag{15}$$

where $\mathcal{L}_{\gamma\gamma}$ is the photon flux in the electron, $W_{\gamma\gamma}$ is the center of mass energy in the $\gamma\gamma$ system, Q_i is the virtuality of photon i and $\sigma_{\gamma\gamma\to b\bar{b},c\bar{c}X}$ is the cross section for the subprocess $\gamma\gamma \to b\bar{b}, c\bar{c}X$.

The direct and single resolved cross sections for b and c quark production in e^+e^- collisions were calculated with CASCADE and compared with the results in [30]. Since the direct cross section is independent of the gluon content in the photon, and hence independent of evolution equations, these cross sections should agree. In heavy flavour production, CASCADE uses off-shell matrix elements as calculated in [25]. Errors were found in [25] (eq. B16) where a factor $N_c e_q^2$ was missing in the direct cross section ($N_c = 3$ being the color factor and e_q being the EM charge of the produced quarks). With these factors taken into account, the direct cross sections from CASCADE and from leading and next-to-leading order calculations [30] were in good agreement, see Table 1. For the single resolved case, the DGLAP evolution was used with the gluon density according to GRV[5] to describe the photon structure and with cuts and parameters as in [30]. As seen, also these cross sections where in good agreement. The aim of this comparison is just to show that the basic machinery for cross section calculations in CASCADE is working.

[5]GRV-G 1HO was used, as in [30]

CHARM

$\sqrt{s}$	$\sigma_{DIR}(pb)$		$\sigma_{1-RES}(pb)$	
(GeV)	*DREES*	*CASCADE*	*DREES*	*CASCADE*
180	296.8 (396.3)	328	269.9 (305.8)	217
91.2	191.2 (254.8)	213	93.38 (109.5)	80

BEAUTY

$\sqrt{s}$	$\sigma_{DIR}(pb)$		$\sigma_{1-RES}(pb)$	
(GeV)	*DREES*	*CASCADE*	*DREES*	*CASCADE*
180	1.280 (1.582)	1.35	1.371 (1.644)	1.19
91.2	0.663 (0.823)	0.71	0.302 (0.371)	0.27

Table 1: *Direct and single resolved charm and beauty cross sections calculated with CASCADE and compared to leading and next-to-leading order (in parenthesis) calculations in [30] (DREES). Here, $\mu^2 = 2m^2$, $\Lambda = 0.34$ GeV, $m_b = 4.75$ GeV and $m_c = 1.6$ GeV. In CASCADE, the scale factor 0.5 was used to obtain the correct scale.*

7.1 e^+e^- cross sections at LEP

In Figure 8a are shown the obtained cross sections for b and c quark production in e^+e^- collisions calculated with the k_t-factorization approach, using off-shell matrix elements and a CCFM unintegrated gluon density evolved from a starting distribution given by GRV, compared to the collinear (DGLAP) predictions and data [1, 2, 7, 8, 9, 10]. Here, the masses $m_b = 4.5, 4.75, 5$ GeV and $m_c = 1.3, 1.5, 1.7$ GeV were used for the CCFM cross sections, while $m_b = 4.75$ GeV and $m_c = 1.5$ GeV were used for the cross sections calculated with DGLAP. This variation of the quark masses gives an estimate of the uncertainty in the calculation. One can see that the k_t-factorization approach describes the charm data reasonably well and that it gives larger cross sections compared to the collinear method. One can also see that the choice of mass makes a significant difference, such that a smaller mass gives a larger cross section. Nevertheless, the cross sections obtained with 1.3 GeV$< m_c <$ 1.7 GeV all lie within the experimental uncertainties.

The cross sections for $b\bar{b}$ production, on the other hand, are not well described. However, in the CCFM approach, one has to determine carefully the normalization of the cross sections. The reason for this is that the normalization of the unintegrated gluon density does not have to be the same as for the standard gluon densities generated according to the collinear scheme, since the integration is made over different regions (i.e. the integral over dk_t^2 is from 0 to μ^2 in the collinear approach, whereas in the CCFM formalism the integral is over all kinematically allowed k_t^2) and the matrix elements are different. This normalization factor has to be applied to the single and double resolved cross sections, but not to the direct cross section since it is independent of the gluon density. Normalizing the CCFM cross section to the charm data at $\sqrt{s} = 200$ GeV for $m_c = 1.5$ GeV, by applying a normalization factor $n = 1.7$ to the single and double resolved cross sections, gives a much steeper behaviour of the total cross section, as seen in Figure 8b. However, the CCFM predictions are still in good agreement with the charm data at $\sqrt{s} < 200$ GeV.

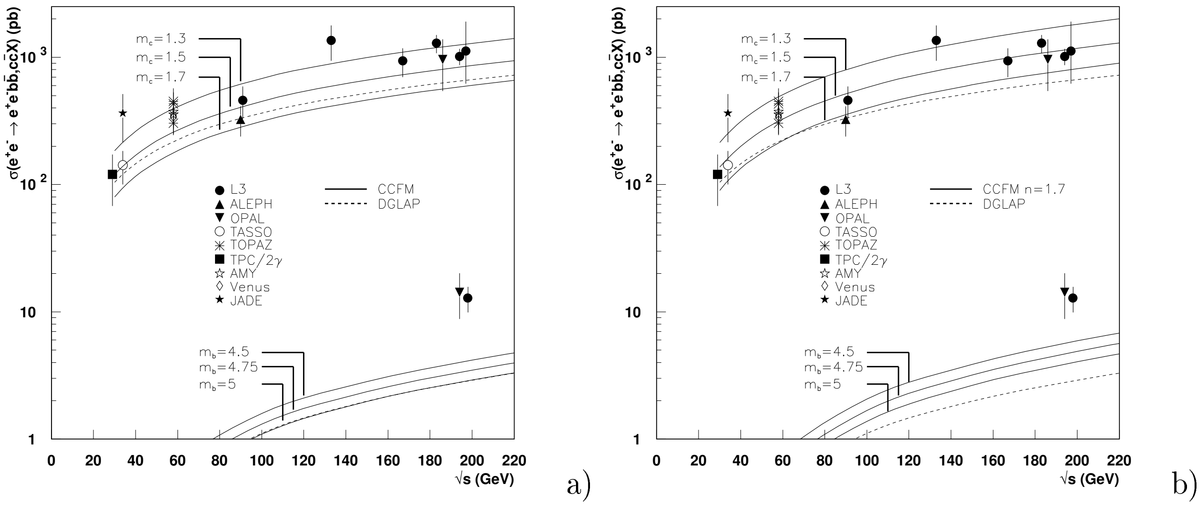

Figure 8: *The charm and beauty cross sections calculated with k_t-factorization compared to the DGLAP approach and data. In (b) the calculated cross section has been normalized to charm data at $\sqrt{s} = 200$ GeV with a factor $n = 1.7$.*

The normalization also improves the situation for the $b\bar{b}$ cross section, where our calculations give $\sigma_{b\bar{b}} = 4.9$ pb at $\sqrt{s} = 200$ GeV. This can be compared to standard collinear NLO predictions which give $\sigma_{b\bar{b}} \approx 4$ pb [7] and results based on [51], giving $\sigma_{b\bar{b}} = 1.9$ pb using a KMR gluon density [52], and $\sigma_{b\bar{b}} = 2.7$ pb using a GBW gluon density [53] at the same energy. The CCFM cross sections are of the same order but a bit larger than NLO standard calculations, which has also been observed in *ep* collisions at HERA. Thus, the improvement is not sufficient fully to describe the $b\bar{b}$ data, which is still a factor 2-3 above predictions.

7.2 e^+e^- and $\gamma\gamma$ cross sections at TESLA

The CCFM predictions for heavy quark production in e^+e^- collisions at TESLA energies are shown in Figure 9a. Here, the normalization factor $n = 1.7$ has been applied for the resolved cross sections. With a charm mass of $m_c = 1.5$ GeV the CCFM predictions at $\sqrt{s} = 500$ (800) GeV are

$$\sigma_{e^+e^- \to e^+e^- c\bar{c}X} = 2770 \ (4165) \text{ pb}.$$

For beauty, the predictions are

$$\sigma_{e^+e^- \to e^+e^- b\bar{b}X} = 17.06 \ (30.72) \text{ pb}$$

using a beauty mass of $m_b = 4.75$ GeV.

Figure 9b shows the charm and beauty cross sections in $\gamma\gamma$ collisions at TESLA energies calculated using the CCFM evolution. The normalization factor $n = 1.7$ has been applied to the resolved contributions. At $\sqrt{s} = 500$ (800) GeV, the predicted cross sections are

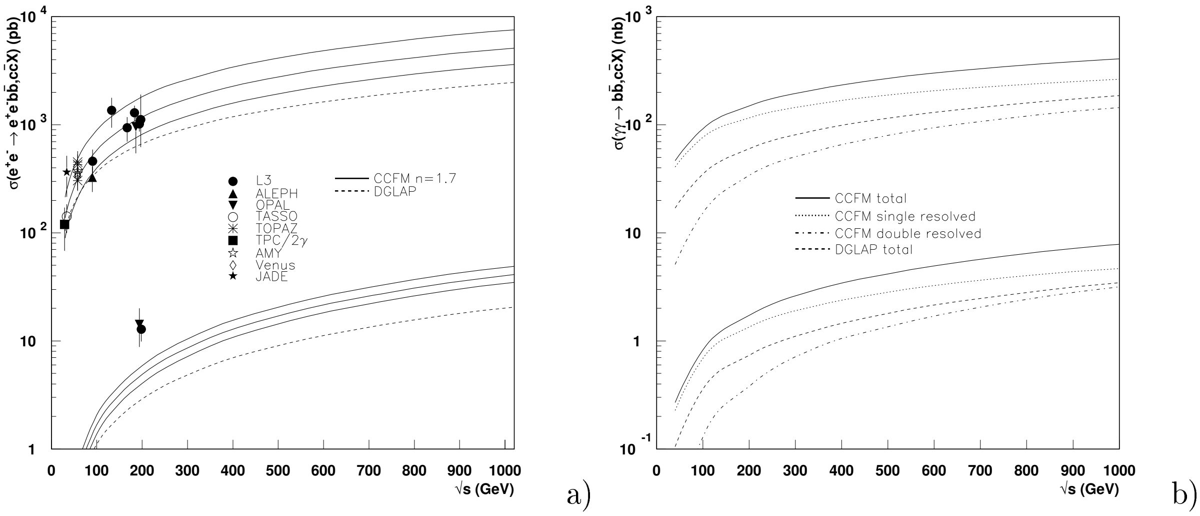

Figure 9: *Heavy quark cross section predictions for (a) e^+e^- and (b) $\gamma\gamma$ collisions at TESLA energies calculated with CCFM and compared to the DGLAP predictions. For CCFM, the quark masses $m_c = 1.3, 1.5, 1.7$ GeV and $m_b = 4.5, 4.75, 5$ GeV were used, where the smallest mass gives the largest cross section. For DGLAP, $m_c = 1.5$ GeV and $m_b = 4.75$ GeV. Also, the normalization factor $n = 1.7$ was applied to the resolved cross sections in the CCFM calculations.*

$$\sigma_{\gamma\gamma\to c\bar{c}X} = 269\ (359)\ \text{nb}$$

for charm and

$$\sigma_{\gamma\gamma\to b\bar{b}X} = 4.18\ (6.38)\ \text{nb}$$

for beauty. Also here, the masses $m_c = 1.5$ GeV and $m_b = 4.75$ GeV were used. Figure 9b also shows the resolved contributions of the cross sections separately. As seen, the single and double resolved cross sections dominate the total cross section at these energies. The reason for this is that the direct contribution, in contrast to the resolved ones, decreases with energy, and is only about 1% of the total cross section at $\sqrt{s} = 100$ GeV.

7.3 Uncertainties

The cross section for heavy quark production depends on the unintegrated gluon density and the partonic cross section. These in turn depend on a few parameters which are not fixed by theory but have to be determined from fits to experimental data, and therefore give rise to some uncertainties in the calculations.

The CCFM evolution of the unintegrated gluon density is sensitive to the input gluon density, the starting scale μ_s and the starting value for the rescaled transverse momentum $\bar{q}_s$. The default values in this analysis are $\mu_s = \bar{q}_s = 1.4$ GeV, obtained from a fit to the parton distribution in the proton [46], with a GRV input distribution. The gluon densities obtained with $\mu_s = 1$ GeV and $\bar{q}_s = 1.4$ GeV, and SaS input distribution with $\mu_s = \bar{q}_s = 1.4$ GeV showed the largest differences compared to the gluon density obtained with the default option (see Figure 6). Therefore, the cross sections were calculated also with these gluon densities to get an estimate of the error.

The strong coupling constant α_s varies with the energy scale μ, according to (in a first approximation)

$$\alpha_s = \frac{12\pi}{(33 - 2 \cdot n_f)\ln(\frac{\mu^2}{\Lambda^2})}. \tag{16}$$

Here, n_f is the number of quark flavours with mass less than the energy scale μ, and Λ is a constant which has to be determined by experiments. The value of Λ also depends on the order that the process is calculated at. However, it is not clear how to compare the value of Λ used in the CCFM approach with the one used in NLO DGLAP, since the first order in the CCFM approach includes some second order diagrams in the DGLAP approach. The default value was chosen to be $\Lambda = 0.2$ GeV, which was also used in the evolution of the unintegrated gluon density, but $\Lambda = 0.34$ GeV (used in [30]) was also tested.

The energy scale μ is of the order of the typical momentum transfer, but the exact choice of scale should be such that the higher order contributions in the perturbative expansion of the cross section are minimal. The standard choice is $\mu^2 = m^2 + p_t^2$, where m is the heavy quark mass and p_t is the transverse momentum of the heavy quarks in the center of mass frame of the heavy quark system. To investigate the effect of the choice of μ, the scale $\mu^2 = 4m^2$ was also used.

The quark masses. Since the quarks are always confined in colorless hadrons, their masses cannot be measured directly. Instead, the masses must be extracted from hadron properties. However, this can be done in various ways depending on the exact definition of the quark masses, and different methods lead to slightly different results. Therefore, the heavy quark masses are varied such that 4.5 GeV $< m_b <$ 5 GeV and 1.3 GeV $< m_c <$ 1.7 GeV. This variation of the quark masses gives the largest uncertainty, and can therefore be used as an estimate of the total uncertainty, as seen in Figure 9, for example.

8 Conclusions

The unintegrated gluon density for the photon was obtained with the full CCFM evolution for the first time. The CCFM evolved gluon density for the photon was used as input in the MC generator CASCADE, and cross sections for heavy quark production in e^+e^- collisions were calculated and compared to LEP data. Also, predictions for charm and beauty production in e^+e^- and $\gamma\gamma$ collisions at TESLA energies are given.

In e^+e^- collisions, the obtained cross sections were somewhat larger than NLO DGLAP predictions, but in good agreement with the charm data from LEP. The CCFM approach made a slight improvement compared to the standard collinear approach for the beauty cross sections. However, the improvement did not fully account for the discrepancy to the $b\bar{b}$ data.

9 Acknowledgements

L.J. would like to thank the organizers for the invitation to give this presentation. This work was supported by INTAS grant 00-00679.

References

[1] D. Buskulic *et al.* (ALEPH Collaboration), *Phys. Lett.* **B 355** (1995) 595

[2] M. Acciarri *et al.* (L3 Collaboration), *Phys. Lett.* **B 453** (1999) 83

[3] M. Acciarri *et al.* (L3 Collaboration), *Phys. Lett.* **B 467** (1999) 137

[4] M. Acciarri *et al.* (L3 Collaboration), *Phys. Lett.* **B 503** (2001) 10

[5] M. Acciarri *et al.* (L3 Collaboration), *Phys. Lett.* **B 514** (2001) 19

[6] M. Acciarri *et al.* (L3 Collaboration), *Phys. Lett.* **B 536** (2002) 217

[7] The L3 Collaboration, L3 Note 2761

[8] The OPAL Collaboration, OPAL Physics Note PN455

[9] G. Abbiendi *et al.* (OPAL Collaboration), *Eur. Phys. J.* **C 16** (2000) 579

[10] G. Altarelli, T. Sjöstrand and F. Zwirner, Physics at LEP2, CERN 96-01 (1996)

[11] TESLA Technical Design Report, DESY 2001-11, TESLA Report 2001-23, TESLA-FEL 2001-05.

[12] P. Jankowski, M. Krawczyk and A. De Roeck, *Eur. Phys. J.* **C 24** (2002) 547

[13] C. Adloff *et al.* (H1 Collaboration), *Nucl. Phys.* **B 545** (1999) 21

[14] C. Adloff *et al.* (H1 Collaboration), *Phys. Lett.* **B 467** (1999) 156; erratum ibid.

[15] C. Adloff *et al.* (H1 Collaboration), *Phys. Lett.* **B 518** (2001) 331

[16] J. Breitweg *et al.* (ZEUS Collaboration), *Eur. Phys. J.* **C 6** (1999) 67

[17] J. Breitweg *et al.* (ZEUS Collaboration), *Eur. Phys. J.* **C 12** (2000) 35

[18] J. Breitweg *et al.* (ZEUS Collaboration), *Eur. Phys. J.* **C 18** (2001) 625

[19] F. Abe *et al.* (CDF Collaboration), *Phys. Rev. Lett.* **71** (1993) 500

[20] F. Abe *et al.* (CDF Collaboration), *Phys. Rev. Lett.* **71** (1993) 2396

[21] F. Abe *et al.* (CDF Collaboration), *Phys. Rev. Lett.* **75** (1995) 1451

[22] B. Abbot *et al.* (D0 Collaboration), *Phys. Lett.* **B 487** (2000) 264

[23] H. Jung, Unintegrated parton densities applied to heavy quark production in the CCFM approach, in *Procedings of the Ringberg workshop on 'New trends in HERA physics', Rinberg Castle, Tegernsee, Germany* (2001), hep-ph/0109146

[24] H. Jung, Heavy quark production at the TEVATRON and HERA using k_t-factorization with CCFM evolution, Lund University, 2001, hep-ph/0110034, DESY 01-136

[25] S. Catani, M. Ciafaloni and F. Hautmann, *Nucl. Phys.* **B 366** (1991) 135

[26] J. Collins and R. Ellis, *Nucl. Phys.* **B 360** (1991) 3

[27] L. Gribov, E. Levin and M. Ryskin, *Phys. Rept.* **100** (1983) 1

[28] E.M. Levin, M.G. Ryskin, Y.M. Shabelski and A.G. Shuvaev, *Sov. J. Nucl. Phys.* **53** (1991) 657

[29] B. Andersson *et al.* (Small x Collaboration), *Eur. Phys. J.* **C 25** (2002) 77

[30] M. Drees *et al.*, *Phys. Lett.* **B 306** (1993) 371

[31] E. Boos, M. Sachwitz, H. J. Schreiber and S. Shichanin, DESY-96-007 *3rd Workshop on Physics and Experiments with* e^+e^- *Linear Colliders (LCWS95), LCWS95: Department Physics: KEK, National Lab for High Energy Physics: 1-1 Oho, Tsukuba-shi: Ibaraki-ken, 305 Japan, 8-12 Sep 1995, Iwate, Japan*

[32] V. Gribov and L. Lipatov, *Sov. J. Nucl. Phys.* **15** (1972) 438 and 675

[33] L. Lipatov, *Sov. J. Nucl. Phys.* **20** (1975) 94

[34] G. Altarelli and G. Parisi, *Nucl. Phys.* **B 126** (1977) 298

[35] Y. Dokshitzer, *Sov. Phys. JETP* **46** (1977) 641

[36] E. Kuraev, L. Lipatov and V. Fadin, *Sov. Phys. JETP* **44** (1976) 443

[37] E. Kuraev, L. Lipatov and V. Fadin, *Sov. Phys. JETP* **45** (1977) 199

[38] Y. Balinsky and L. Lipatov, *Sov. J. Nucl. Phys.* **28** (1978) 822

[39] M. Ciafaloni, *Nucl. Phys.* **B 296** (1988) 49

[40] S. Catani, F. Fiorani and G. Marchesini, *Phys. Lett.* **B 234** (1990) 339

[41] S. Catani, F. Fiorani and G. Marchesini, *Nucl. Phys.* **B 336** (1990) 18

[42] G. Marchesini, *Nucl. Phys.* **B 445** (1995) 49

[43] H. Jung, *Comp. Phys. Comm.* **143** (2002) 100

[44] T. Sjöstrand, *Comp. Phys. Comm.* **82** (1994) 74

[45] G. Ingelman, A. Edin and J. Rathsman, *Comp. Phys. Comm.* **101** (1997) 108

[46] H. Jung and G. P. Salam, *Eur. Phys. J.* **C 19** (2001) 351

[47] B. R. Webber, *Nucl. Phys. Proc. Suppl.* **18C** (1991) 38.

[48] G. Marchesini and B. R. Webber, *Nucl. Phys.* **B 386** (1992) 215.

[49] A. Gawron and J. Kwiecinski, *Acta Phys. Polon.* **B 34** (2003) 133

[50] G. A. Schuler and T. Sjöstrand, *Phys. Lett.* **B 276** (1996) 193

[51] L. Motyka and N. Timneanu, *Eur. Phys. J.* **C 27** (2003) 73

[52] M.A. Kimber, A.D. Martin, M.G. Ryskin, *Phys. Rev.* **D 63** (2001) 114027

[53] K. Golec-Biernat, M. Wüsthoff, *Phys. Rev.* **D 60** (1999) 114023